Latest Alzheimer's Research

Gamma frequency entrainment attenuates amyloid load and modifies microglia
Li-Huei Tsai, PhD, and Ed Boyden, PhD, pioneers in brain research, published a landmark study showing dramatic benefit in treating Alzheimer's using a non-invasive brain stimulation technique. These compelling results are the foundation of the clinical trials we are conducting today.
Abstract

Changes in gamma oscillations (20–50 Hz) have been observed in several neurological disorders. However, the relationship between gamma oscillations and cellular pathologies is unclear. Here we show reduced, behaviourally driven gamma oscillations before the onset of plaque formation or cognitive decline in a mouse model of Alzheimer's disease. Optogenetically driving fast-spiking parvalbumin-positive (FS-PV)-interneurons at gamma (40 Hz), but not other frequencies, reduces levels of amyloid-β (Aβ)1–40 and Aβ 1–42 isoforms. Gene expression profiling revealed induction of genes associated with morphological transformation of microglia, and histological analysis confirmed increased microglia co-localization with Aβ. Subsequently, we designed a non-invasive 40 Hz light-flickering regime that reduced Aβ1–40 and Aβ1–42 levels in the visual cortex of pre-depositing mice and mitigated plaque load in aged, depositing mice. Our findings uncover a previously unappreciated function of gamma rhythms in recruiting both neuronal and glial responses to attenuate Alzheimer's-disease-associated pathology.
Main
Activation of local circuits of excitatory and fast-spiking inhibitory neurons that resonate at 20–50 Hz gives rise to oscillations in the local field potential (LFP), called gamma oscillations[1,2,3]. Although studies have demonstrated disrupted gamma in various neurological diseases, the interplay between pathology and this emergent circuit property has yet to be determined[4,5]. In general, molecular and cellular pathology is thought to alter synaptic activity. However, in at least one disorder, Alzheimer's disease (AD), changes in synaptic activity can also feedback to alter molecular pathology. Studies have shown that increases in synaptic activity in vivo increase levels of Aβ[6], a 36- to 43-amino-acid protein, whose aggregation is thought to initiate neurotoxic events, including neuroinflammation, synaptic and neuronal loss, and tau-associated pathology[7]. We aimed to determine how gamma affects molecular pathology in a mouse model of AD. Understanding how gamma might affect disease pathogenesis has important implications for elucidating both the basic pathology of and possible therapeutic interventions for neurological diseases with altered gamma.
Reduced hippocampal gamma in 5XFAD mice Reduced hippocampal gamma in 5XFAD mice
Altered gamma has been observed in multiple brain regions in several neurological and psychiatric disorders, including a reduction in spontaneous gamma synchronization in patients with AD and reduced gamma power in multiple AD mouse models[4,5,8,9]. However, it is unclear whether gamma is altered early in disease progression and whether it affects disease pathology. Accordingly, we recorded neural activity from behaving 5XFAD mice, a well-established model of AD[10]. In 3-month-old mice, which have elevated levels of Aβ but no major plaque accumulation in the hippocampus or manifestation of learning and memory deficits[10], we recorded neural activity from hippocampal subregion CA1, where gamma has been particularly well characterized (see, for example, refs 11, 12, 13, 14), using a virtual environment (Extended Data Fig. 1a). In CA1, gamma is present during distinct periods of activity: running, when theta oscillations (4–12 Hz) occur (Extended Data Fig. 1b, left); and quiescent behaviour, when sharp-wave ripples (SWRs) occur[15,16] (Extended Data Fig. 1b, right). We found no clear differences in slow gamma power (20–50 Hz) between 5XFAD mice and wild-type (WT) littermates during theta (Extended Data Fig. 1c, d).

We next examined gamma during SWRs, high-frequency oscillations of 150–250 Hz lasting around 50–100 ms (Extended Data Fig. 1b, e)[14]. Previous work has shown that slow gamma is elevated during SWRs and that increased gamma synchrony across CA3 and CA1 during SWRs correlates with more coordinated firing between neurons[16]. Similarly, we found increased gamma power during SWRs (Fig. 1a, a yellow arrow indicates elevated gamma, and Extended Data Fig. 1e). The instantaneous

frequencies of these slower oscillations (10–50 Hz, Methods) were a unimodal distribution centred around 40 Hz (Fig. 1b and Extended Data Fig. 1f). Comparing gamma during SWRs in WT and 5XFAD littermates, we found that gamma power was significantly lower in 5XFAD than in WT mice (Methods, Fig. 1c and Extended Data Fig. 1g, j; examples in Fig. 1c, top). Spiking was phase-modulated by gamma in both groups, although the depth of modulation was significantly smaller in 5XFAD than in WT animals (Fig. 1d and Extended Data Fig. 1h, k). Furthermore, there were fewer SWRs per unit time in non-theta periods in 5XFAD mice compared with WT (Extended Data Fig. 1i), reducing periods when gamma power is elevated (Fig. 1a, c and Extended Data Fig. 1e). These results reveal deficits in gamma modulation of CA1 spiking in a mouse model of AD before the development of major amyloid plaque accumulation or evidence of cognitive impairment. This deficit in gamma converges with evidence of gamma deficits in different mouse models of AD, and reports that gamma is altered in humans with AD[5,8,9]. Indeed, molecular deficits in Nav1.1 in humans have been linked with gamma deficits in hAPP mice[7].

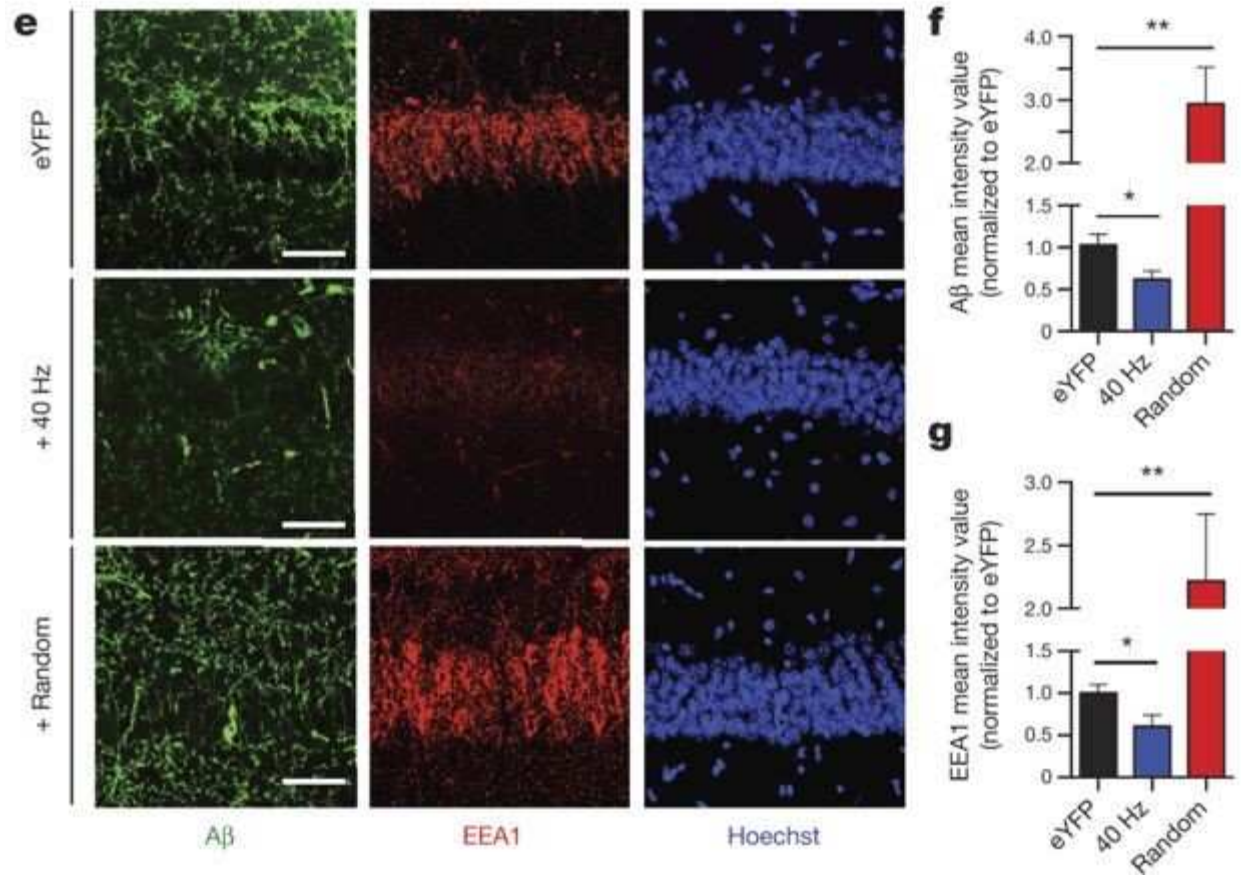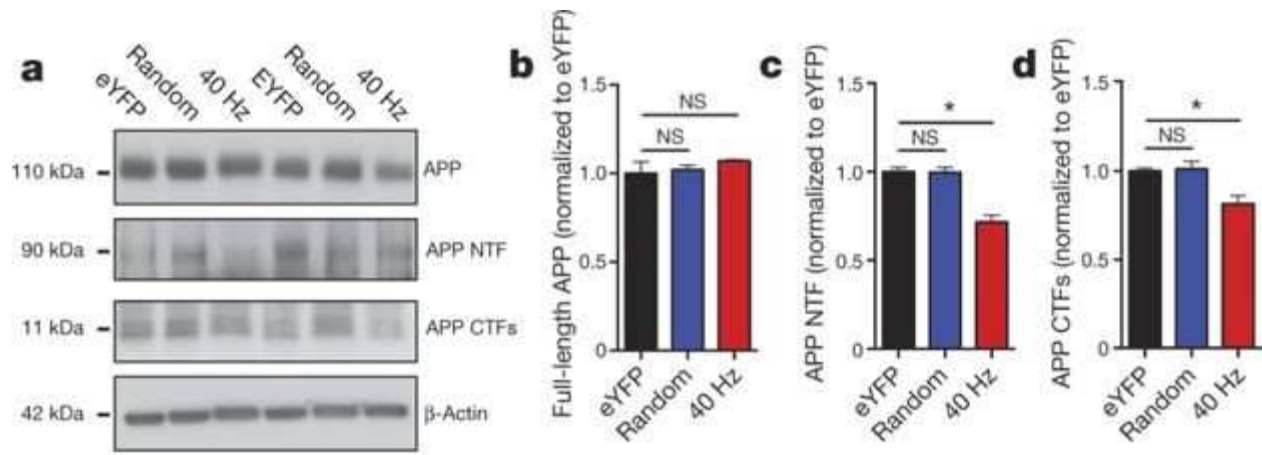Figure 1: 5XFAD mice have reduced power in gamma during hippocampal SWRs.
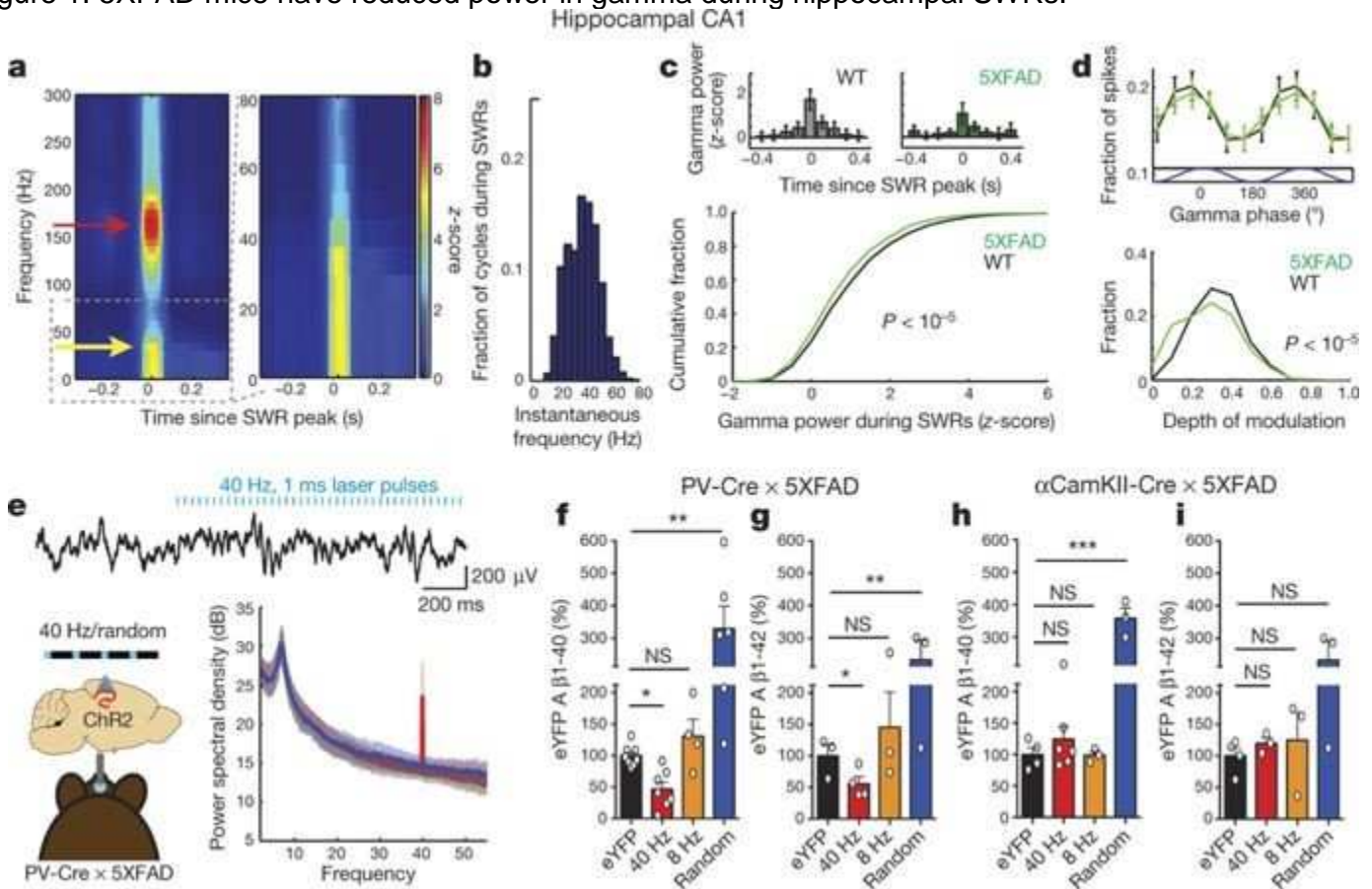
a, Average SWRs-triggered spectrograms for one mouse (left) showing gamma (yellow arrow) during SWRs (red arrow); right: frequencies below 80 Hz enlarged (n = 370 SWR). b, Histogram of instantaneous gamma frequencies during SWRs for mouse in a. c, Above: z-scored gamma power around SWR peaks for one WT and one 5XFAD mouse (mean ± s.e.m.). Below: cumulative distribution of gamma power during SWRs (rank-sum test, n = 2,166 and 3,085 SWRs in six 5XFAD and WT mice, respectively). d, Above: fraction of spikes during SWRs as a function of gamma phase (mean ± s.e.m.). Below: depth of gamma spiking modulation during SWRs (rank-sum test, bootstrap resampling, n = 2,500 5XFAD and 3,000 WT phase distributions). e, Above: LFP trace before and during 40 Hz optogenetic stimulation. Below: mean and standard deviation of power spectral density (n = 4 5XFAD and 3 WT mice). Red, 40 Hz; blue, random; black, no stimulation.f, Relative Aβ1–40 levels in CA1 of 5XFAD/PV-Cre mice in each stimulation condition normalized to eYFP controls (n = 8 eYFP, n = 7 40 Hz, n = 4 8 Hz, n = 6 random mice). g, As in f for Aβ1–42 (n = 4 eYFP, n = 4 40 Hz, n = 3 8 Hz, n = 3 random mice). h, Relative Aβ1–40 levels in CA1 of 5XFAD/αCamKII-Cre mice in each stimulation condition normalized to eYFP controls (n = 6 40 Hz, n = 3 8 Hz, n = 3 random mice). i, As in h for Aβ1–42 (n = 3 mice per group). NS, not significant, *P < 0.05, **P < 0.01, ***P < 0.001 by one-way analysis of variance (ANOVA); circles indicate n, mean + s.e.m. unless otherwise specified in bar graphs.

Gamma reduced Aβ production in CA1Gamma reduced Aβ production in CA1

These gamma deficits during SWRs early in disease progression in this mouse model of AD prompt the question of whether gamma could affect molecular and cellular AD pathophysiology. To test this, we induced gamma optogenetically in 5XFAD/PV-Cre mice (Methods, Fig. 1e, left, and Extended Data Fig. 2a–c). We chose to drive FS-PV-interneurons at 40 Hz because we found deficits in gamma during SWRs, and instantaneous gamma frequencies during SWRs were centred around 40 Hz. Delivering 1 ms, 473 nm light pulses at 40 Hz resulted in increased power at 40 Hz in LFPs in CA1, while random stimulation did not (Fig. 1e and Extended Data Fig. 1l). Both resulted in similar firing rates (Extended Data Fig. 1m–o).

Aβ accumulation is thought to initiate multiple neurotoxic events typical for AD pathology. Therefore, we examined whether gamma stimulation affected overall Aβ peptide levels in the hippocampus of 5XFAD mice. We found that 1 h of FS-PV-interneuron stimulation reduced Aβ1–40 by 53.22% and Aβ1–42 by 44.62% in the 40 Hz group, which expresses ChR2 compared with the enhanced yellow fluorescent protein (eYFP) control group, as measured in CA1 by Aβ enzyme-linked immunosorbent assay (ELISA) (Fig. 1f, g and raw concentration (picograms per millilitre) in Extended Data Table 1). We performed a comprehensive set of control experiments to determine whether the effect was specific to frequency, cell type, and/or rhythmicity. Neither stimulation of CamKII-positive excitatory neurons at 40 Hz nor FS-PV-interneurons at 8 Hz or random intervals significantly reduced Aβ levels (Fig. 1f–i and Methods). Immunohistochemical analysis using two β-amyloid-specific antibodies (Cell Signalling Technology; D54D2, BioLegend; 12F4 (ref. 17)) in CA1 confirmed these results: Aβ labelling intensity was significantly reduced by 39.5% after 40 Hz stimulation compared with eYFP controls (Fig. 2e, f, D54D2 antibody; Extended Data Fig. 2e, f, 12F4 antibody).

Figure 2: Driving 40 Hz oscillations optogenetically in hippocampus reduces Aβ in 5XFAD mice.

a

110 kDa — APP
90 kDa — APP NTF
11 kDa — APP CTFs
42 kDa — β-Actin

eYFP Random 40 Hz EYFP Random 40 Hz

b Full-length APP (normalized to eYFP)

NS
NS

eYFP Random 40 Hz

c APP NTF (normalized to eYFP)

*
NS

eYFP Random 40 Hz

d APP CTFs (normalized to eYFP)

*
NS

eYFP Random 40 Hz

e

eYFP

+ 40 Hz

+ Random

Aβ   EEA1   Hoechst

f Aβ mean intensity value (normalized to eYFP)

**
*

eYFP 40 Hz Random

g EEA1 mean intensity value (normalized to eYFP)

**
*

eYFP 40 Hz Random

a, Representative western blot showing levels of APP (CT695), APP NTF (A8967), APP CTFs (CT695), and β-actin (A5316, loading control) in CA1 of 5XFAD/PV-Cre mice expressing only eYFP or ChR2 with 40 Hz, or random stimulation conditions. One mouse per lane, two biological replicates. b, Relative immunoreactivity of full-length APP normalized to actin (for b–d, n = 6 mice per group). c, Relative immunoreactivity of APP NTF normalized to actin. d, Relative immunoreactivity of APP CTFs normalized to actin. e, Immunohistochemistry with anti-Aβ(D54D2, green) and anti-EEA1 (610457, red) antibodies in CA1 of 5XFAD/PV-Cre mice (scale bar, 50 μm). f, Relative immunoreactivity of Aβ normalized to eYFP controls (for f, g, n = 3 mice per group). g, Relative immunoreactivity of EEA1 normalized to eYFP controls. *P < 0.05, **P < 0.01, by one-way ANOVA; mean + s.e.m. in bar graphs.

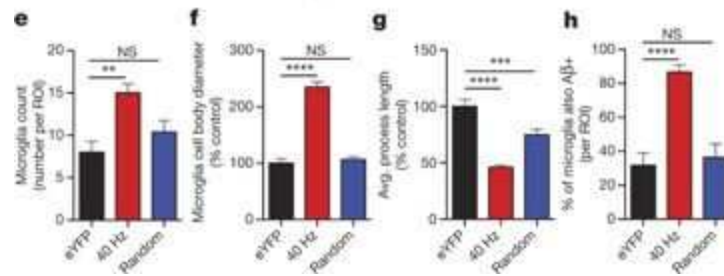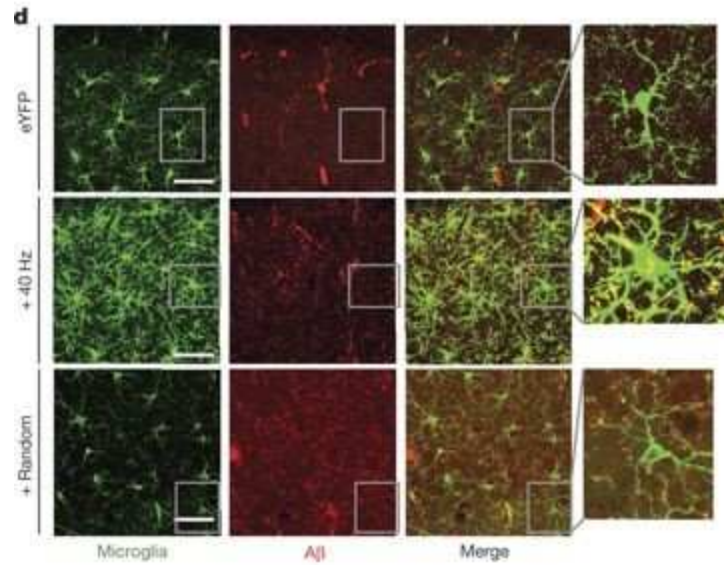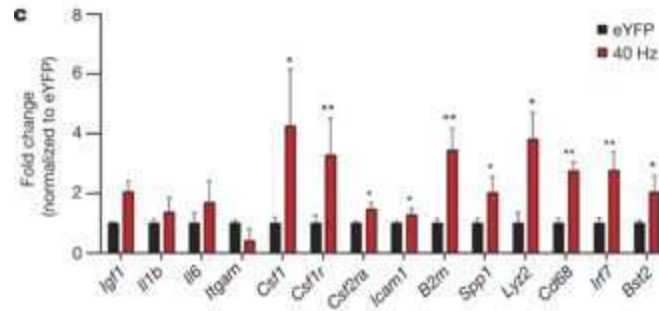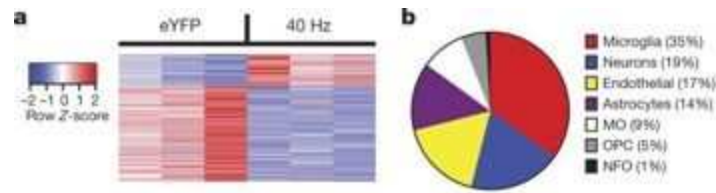Brain amyloid concentration depends on Aβ production from amyloid precursor protein (APP) and Aβ clearance rates. To elucidate whether 40 Hz stimulation reduced Aβ production, we examined its effects on APP cleavage by measuring levels of the cleavage intermediates of APP, C-terminal fragments (CTFs) and amino (N)-terminal fragments (NTF), in the hippocampus of the 5XFAD/PV-Cre mice. After 40 Hz stimulation, we found significantly reduced APP CTFs and NTF compared with eYFP and random controls (Fig. 2a–d and Extended Data Fig. 2d).

Previous work has shown that APP is transported and processed in recycling endosomes[18], and enlarged early endosomes have been observed in brain tissue from patients with AD[19]. Therefore, we characterized endosomes in CA1 after stimulation using two markers, EEA1 (early endosomal antigen 1) and Rab5 (Ras-related protein encoded by the RAB5A gene). Altogether, the intensity of endosomal labelling of CA1 neurons significantly decreased in both EEA1 (39.7%) and Rab5 (40.1%) after 40 Hz stimulation compared with eYFP controls (Fig. 2e, g and Extended Data Fig. 2g, h). These results suggest that, in addition to observed changes in APP cleavage products, 40 Hz stimulation also alters general endosomal processing.

Gamma induced microglia morphological changesGamma induced microglia morphological changes

To explore further the cellular and molecular effects of stimulation in an unbiased manner, we performed genome-wide RNA sequencing (RNA-seq) of CA1 tissue after 1 h of 40 Hz or no stimulation (eYFP) of the 5XFAD/PV-Cre mice (Fig. 3a and Extended Data Fig. 3a, b, c). Notably, 35% of all upregulated genes had their highest expression in microglia (Fig. 3b). This RNA-seq analysis strongly suggests that 40 Hz stimulation causes an alteration in the state of microglia, which is noteworthy given the accumulating evidence that microglia play a role in AD pathology[20]. Transcriptomic changes after 40 Hz stimulation were positively correlated with changes due to increased neural activity (by NMDA (N-methyl-d-aspartate) and bicuculline), and negatively correlated with changes due to silencing activity (by tetrodotoxin) (Extended Data Fig. 3d). The immediate early genes Nr4a1, Arc, and Npas4, which are upregulated by neuronal activity, were elevated as shown by both RNA-seq and reverse transcribed quantitative PCR (RT-qPCR) (Extended Data Fig. 3e).

Figure 3: Driving 40 Hz oscillations optogenetically in hippocampus causes a distinct morphological transformation of microglia in 5XFAD mice.

a

eYFP   40 Hz

Row Z-score
−2 −1 0 1 2

b

- Microglia (35%)
- Neurons (19%)
- Endothelial (17%)
- Astrocytes (14%)
- MO (9%)
- OPC (5%)
- NFO (1%)

c

■ eYFP
■ 40 Hz

Fold change (normalized to eYFP)

Igf1 Il1b Il6 Itgam Csf1 Csf1r Csf2ra Icam1 B2m Spp1 Lyz2 Cd68 Irf7 Bst2

d

eYFP

+ 40 Hz

+ Random

Microglia   Aβ   Merge

e

Microglia count (number per ROI)

NS
**

eYFP 40 Hz Random

f

Microglia cell body diameter (% control)

NS
****

eYFP 40 Hz Random

g

Avg. process length (% control)

***
****

eYFP 40 Hz Random

h

% of microglia also Aβ+ (per ROI)

NS
****

eYFP 40 Hz Random

a, Heat map of differentially expressed genes determined by whole-transcriptome RNA-Seq of CA1 from 5XFAD/PV-Cre mice expressing only eYFP or ChR2 with 40 Hz stimulation. Normalized z-score values (high: red; low: blue) were calculated for each differentially expressed gene (row). b, Cell-type-specific expression patterns of upregulated genes after 40 Hz stimulation (MO, myelinating oligodendrocyte; OPC, oligodendrocyte progenitor cell; NFO, newly formed oligodendrocyte). c, RT-qPCR of specific upregulated genes: relative RNA levels (fold change) in CA1 of 5XFAD/PV-Cre expressing only eYFP or ChR2 with 40 Hz stimulation, normalized to eYFP controls (Student's t-test; n = 6 mice per group). d, Immunohistochemistry with anti-Iba1 (019-19741, green) to identify microglia and anti-Aβ (12F4, red) antibodies in CA1 of 5XFAD/PV-Cre mice expressing only eYFP or ChR2 with 40 Hz, and random stimulation (40× objective; scale bar, 50 μm). e, Number of Iba1-positive microglia (for f–i, one-way ANOVA; n = 4 mice per group). f, Diameter of Iba1-positive microglia cell bodies. g, Average length of Iba1-positive microglia primary processes. h, Percentage of Iba1-positive microglia cell bodies that are also Aβ-positive. *P < 0.05, **P < 0.01, ***P < 0.001, ****P < 0.0001; mean + s.e.m. in bar graphs.

These transcriptomic results also suggest an engulfing state of microglia. The upregulated genes were positively correlated with gene expression changes induced by macrophage colony-stimulating factor and granulocyte macrophage colony-stimulating factor, known to promote microglial Aβ uptake[21] (Extended Data Fig. 3d). RT-qPCR confirmed that upregulated genes included microglial engulfment associated genes Cd68, B2m, Bst2, Icam1, and Lyz2 (Fig. 3c). Microglia-enriched transcriptional regulator Irf7, cell adhesion and migration regulator Spp1, and microglia proliferation markers Csf1r and Csf2ra were also upregulated (Fig. 3c). Notably, RT-qPCR showed that the expression levels of pro-inflammatory genes Il6, Il1b (Il1-β), Itgam (Cd11b), and the anti-inflammatory gene Igf1 were not changed (Fig. 3c).

Given that 40 Hz stimulation upregulated both phagocytosis- and migration/cell adhesion-related genes, we examined morphological features of microglia activation. We used an antibody against microglial marker Iba1 to label microglia in CA1 sections from 5XFAD/PV-Cre mice after 1 h of 40 Hz or random stimulation, or in mice expressing only eYFP (Fig. 3d). We observed almost twice as many microglia in the 40 Hz group compared with the eYFP and random control groups (Fig. 3d, e). Furthermore, microglia cell body diameter increased by 135.3% after 40 Hz stimulation compared with eYFP controls and by 138.7% compared with random stimulation (Fig. 3d, f). The lengths of microglia primary processes were reduced by 54.0% in the 40 Hz stimulation condition compared with eYFP controls and by 38.5% compared with random stimulation (Fig. 3d, g). Iba1 levels did not affect these findings, as gene expression analysis showed that Iba1 expression did not differ between conditions (Extended Data Fig. 3a, b). The increase in cell body size and decrease in process length observed after 40 Hz stimulation are consistent with a shift towards a phagocytic state of microglia[22]. To evaluate microglia Aβ uptake specifically, we measured co-localization of Aβ within microglia by co-immunostaining with an Aβ antibody (12F4, Methods). The percentage of microglia co-localized with Aβ in the cell body increased to 85.6% after 40 Hz stimulation from 31.7% (eYFP control, Fig. 3d, h). Three-dimensional renderings of microglia further demonstrated the presence of Aβ within microglia (Supplementary Videos 1,2,3). We did not find evidence of neuronal loss by measuring the CA1 cellular layer thickness (Extended Data Fig. 3f, g). Together, these results suggest that gamma stimulation triggers microglia to increase Aβ uptake.
Light flicker entrains gamma in VCLight flicker entrains gamma in VC

Many studies have shown that visual stimulation can drive oscillations in the gamma range[2,23]. In particular, flickering lights at a specific frequency can induce that frequency in primary visual cortex (VC)[24]. To determine whether light flickering could entrain 40 Hz oscillations to subsequently alter Aβ, we exposed 5XFAD mice to 40 Hz flickering for 1 h, analogous to optogenetic stimulation that reduced Aβ

described above (Supplementary Video 4 and Methods). In VC, we found that light flickering at 40 Hz increased power in the LFP at 40 Hz, while random interval flickering (random flicker) and dark exposure did not (Fig. 4a and Extended Data Fig. 4a). All induced similar firing rates (Extended Data Fig. 4b, c). Spiking increased and decreased concomitantly as the light flickered on and off, resulting in spiking entrained to 40 Hz during 40 Hz flicker but not during random flicker (Fig. 4b). Recordings from saline above the brain exhibited no change in 40 Hz power during 40 Hz flicker, showing that this effect was not due to photoelectric effects or electrical noise (Extended Data Fig. 4d, e).

Figure 4: Driving 40 Hz oscillations in VC via light flicker reduces Aβ and amyloid plaques in 5XFAD mice.
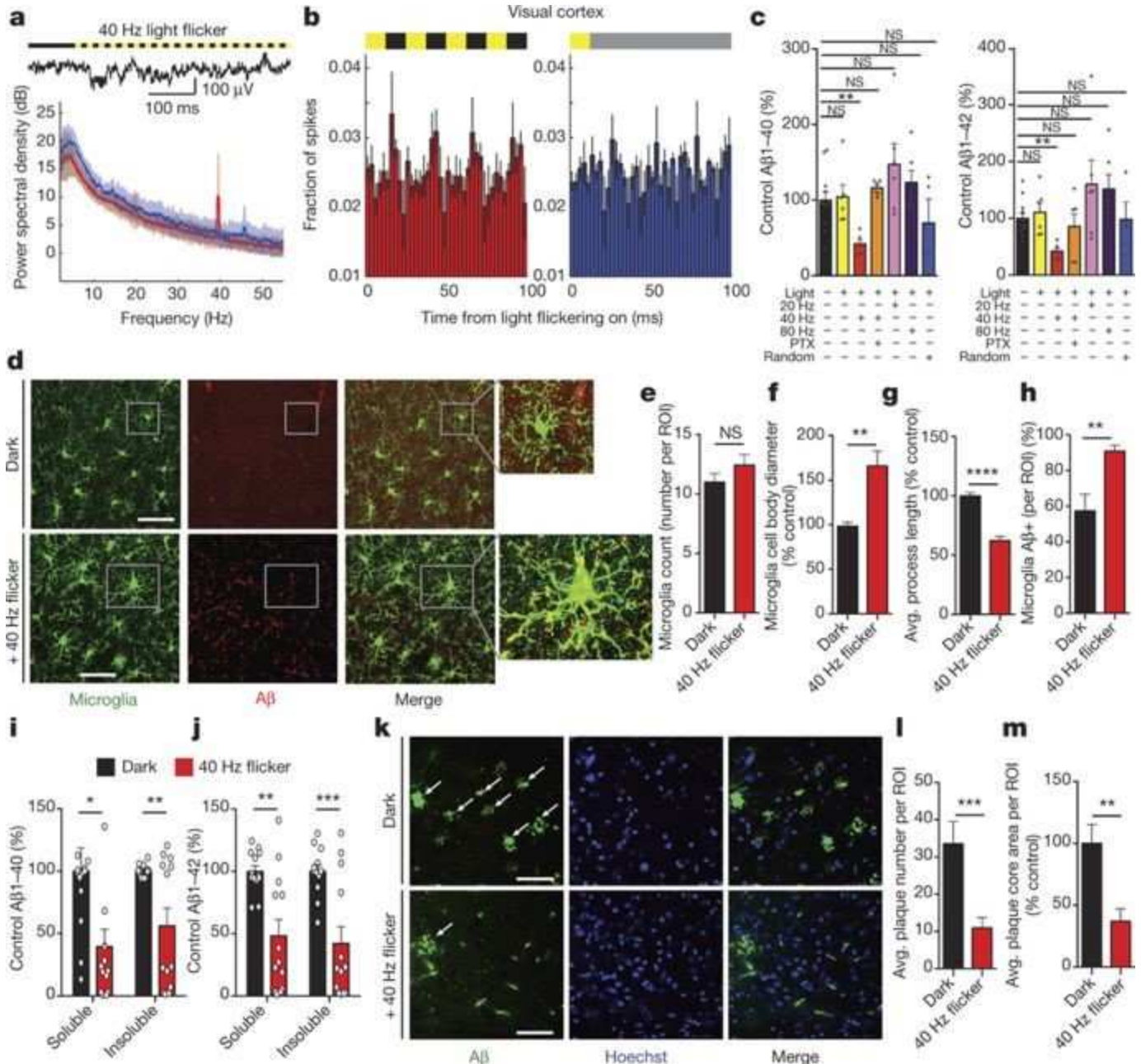
a, LFP trace in VC before and during 40 Hz light flicker (above). Power spectral density mean and s.d. (below, n = 4 5XFAD mice, five recording sessions). b, Fraction of spikes in VC over four cycles of 40 Hz flicker (left) or the equivalent time for random flicker (right, n = 4 5XFAD mice from five recording sessions, mean ± s.e.m. across animals). For random stimulation, spiking was aligned to light turning on; grey indicates additional light-on flickers occurring randomly (Methods). c, Relative Aβ1–40 (left) and Aβ1–42 (right) levels normalized to dark, in VC of 5XFAD mice exposed to dark, light, 40 Hz, 20 Hz, 80 Hz, 40 Hz with picrotoxin (PTX), and random conditions (n = 12 dark; n = 6 light, 40 Hz, 20 Hz, 80 Hz flicker and PTX; n = 4 random mice; one-way ANOVA). d, Immunohistochemistry with anti-Iba1 (019-19741, green) and anti-Aβ(12F4, red) antibodies in VC of 5XFAD mice exposed to dark or 40 Hz flicker. Right: 120× zoom; arrows indicate +Iba1/+Aβ signal in cell body (scale bar, 50 μm). e, Number of Iba1-positive microglia (for e–h Student's t-test unpaired, n = 4 mice per group). f, Diameter of Iba1-positive microglia cell bodies. g, Average length of Iba1-positive microglia primary processes. h, Percentage of Iba1-positive microglia cell bodies that are also Aβ-positive. i, Relative Aβ1–40 levels in VC of 6-month-old 5XFAD mice after 7 days of 1 h per day dark or 40 Hz flicker (Student's t-test unpaired; n = 13 mice per group). j, As in i for Aβ1–42. k, Immunohistochemistry with anti-Aβ (D5452, green) antibody in 6-month-old VC of 5XFAD mice after 7 days of 1 h per day dark or 40 Hz flicker showing plaques (white arrows; scale bar, 50 μm). l, Number of Aβ-positive plaques; (for l, m, Student's t-test unpaired, n = 8 mice per group). m, Area of Aβ-positive plaques. *P < 0.05, **P < 0.01, ***P < 0.001; circles indicate n, mean + s.e.m. in bar graphs.

Given that 40 Hz light flicker entrains 40 Hz oscillations in VC, we aimed to determine whether 40 Hz flicker could reduce Aβ levels. Three-month-old 5XFAD mice were placed in a dark box and exposed to either light flicker at different frequencies (20, 40, or 80 Hz), random flicker, constant light-on (light), or dark for 1 h. One hour after 1 h of 40 Hz flicker, we observed that Aβ1–40 levels in VC were reduced by 57.96% and Aβ1–42 levels by 57.97% compared with dark controls (as measured by Aβ ELISA, Fig. 4c). The effect was specific to 40 Hz flicker as neither constant light nor 20 Hz, 80 Hz, or random flicker significantly reduced Aβ levels compared with dark and light controls (Fig. 4c). We also found no change in Aβ levels in somatosensory barrel cortex and hippocampus after 40 Hz flicker (Extended Data Fig. 5a–h). When we pre-treated 5XFAD mice with a low-dose of GABAA antagonist (picrotoxin, 0.18 mg/kg (ref. 25)), the effects of 40 Hz flicker on Aβ levels were completely abrogated, indicating that GABAergic neurotransmission is necessary for this effect (Fig. 4c). To demonstrate that these effects extend beyond the 5XFAD mouse, we examined the effect of 40 Hz flicker in APP/PS1 mice, another well-validated AD model26, and found significantly reduced Aβ1–40, by 20.80%, and a non-significant trend of reduced Aβ1–42 by 37.68% (Extended Data Fig. 6a). Furthermore, in 9-month-old WT mice, we found a 58.2% reduction in endogenous mouse Aβ1–40 after 1 h of 40 Hz flicker (Extended Data Fig. 6b). The reduction of endogenous mouse Aβ1–40 in WT animals reveals that these effects are not restricted to transgenic APP expression or mutant APP; rather, they extend to Aβ produced from endogenous APP driven by its endogenous promoter.

Next, we investigated whether 40 Hz flicker alters microglia activity in VC in a similar manner to the way 40 Hz optogenetic stimulation altered CA1 microglia. While microglia number was unchanged (Fig. 4d, e), microglia cell body diameter increased by 165.8% after 40 Hz flicker compared with dark controls (Fig. 4d, f). Microglia primary process lengths were reduced by 37.7% after 40 Hz flicker compared with dark controls (Fig. 4d, g). Consistent with this morphology, which indicates enhanced engulfment activity22, Aβ/Iba1 co-localization in the cell body was increased to 90.8% after 40 Hz flicker from 57.3% in the dark condition, indicating more Aβ-bearing microglia (Fig. 4d, h, P < 0.01). To better resolve the morphological change in microglia, we used CLARITY27 to create three-dimensional renderings of microglia from 100 μm sections of VC (Supplementary Videos 5, 6). To demonstrate that microglia indeed engulf Aβ in

the 5XFAD mouse, we purified microglia from 5XFAD and WT animals using fluorescence-activated cell sorting (FACS) and analysed Aβ levels via human ELISA. We found that microglia-specific levels of Aβ are significantly higher in 5XFAD animals than in WT controls (Extended Data Fig. 7a, b). Synaptophysin levels did not change between dark and 40 Hz flicker conditions, indicating that microglia activation probably did not affect synapse number (Extended Data Fig. 7c, d; NS, not significant, n = 4 mice). Thus, 40 Hz oscillations induced non-invasively via sensory entrainment reduced Aβ abundance and promoted microglia/Aβ interactions.

We next assessed whether 40 Hz flicker was effective in treating animals that have amyloid plaques. Because the effects of 40 Hz flicker on soluble Aβ levels were transient, lasting 12 h but not 24 h (Extended Data Fig. 8a), we hypothesized that we would need repeated exposure to affect insoluble Aβ. Thus, we treated 6-month-old 5XFAD mice, which have amyloid plaque pathology in many brain regions including VC10, for 1 h daily over 7 days with 40 Hz flicker or dark, and analysed VC tissue 24 h later. We found that 7 days of 1 h 40 Hz flicker reduced both soluble Aβ1–40 and Aβ1–42 levels, by 60.5% and 51.7% respectively, (Fig. 4i, j) and insoluble Aβ1–40 and Aβ1–42 levels by 43.7% and 57.9% respectively (Fig. 4i, j). Immunohistochemical analysis showed that 40 Hz flicker significantly reduced plaque number in VC by 67.2% compared with dark controls (Fig. 4k, l) and plaque size by 63.7% (Fig. 4k, m). Taken together, these experiments identify a non-invasive treatment with a profound effect on amyloid plaque pathology. We next determined if 40 Hz flicker reduced tau phosphorylation by immunohistochemistry, another AD-related pathology. Using the TauP301S tauopathy mouse model28 we found that 7 days of 1 h 40 Hz visual flicker treatment reduced phosphorylated tau serine202 and serine404/threonine403/serine400 levels in VC by 41.2% and 42.3%, respectively, and triggered microglia responses similar to those observed in 5XFAD mice (Extended Data Fig. 9a–k).

Gamma oscillations are thought to be important for higher cognitive functions and sensory responses2,12,23. Here, we demonstrated that entraining oscillations and spiking at 40 Hz, using optogenetics in the hippocampus of 5XFAD mice and using a non-invasive light flicker treatment to affect primary VC in multiple mouse models, resulted in a marked reduction of Aβ peptides. We also found a concomitant microglia response after 40 Hz entrainment.

The robust reduction of total amyloid levels was probably mediated both by decreased amyloidogenesis and by increased amyloid endocytosis by microglia. Thus, it appears that driving 40 Hz gamma oscillations may induce an overall neuroprotective response that recruits both neurons and microglia. The fact that GABAA antagonist treatment completely abrogated the effects of 40 Hz stimulation on Aβ levels strongly suggests that GABAergic neurotransmission is critical for these effects.

Flicker stimulation at 40 Hz reduced Aβ in multiple mouse models, including 5XFAD, APP/PS1, and WT mice. This replication in multiple mouse models shows that these findings are not specific to one animal model and, importantly, extend to situations where Aβ is produced from APP expressed by its physiological promoter as it is in WT animals. In addition, we found that 40 Hz oscillations reduced phosphorylated tau staining in a mouse model of tauopathy, TauP301S, showing that the protective effects of gamma stimulation generalize to other pathogenic proteins.

These observations indicate that entraining gamma oscillations may provide a broad spectrum of systemic effects in the brain, including in non-neuronal cells, to attenuate AD-related pathology. Because this approach is fundamentally different from previous AD therapies29, further study is needed to determine whether it will be therapeutic in human AD.

Methods

All animal work was approved by the Committee for Animal Care of the Division of Comparative Medicine at the Massachusetts Institute of Technology. Adult (3-month-old) male double transgenic 5XFAD Cre mice were produced by crossing 5XFAD transgenic mice with the transgenic PV or CW2 promoter driven Cre line. Adult (5-month-old) male and female APP/PS1 mice were gifted from the Tonegawa laboratory. Adult (4-month-old) male TauP301S mice were obtained from the Jackson Laboratory. Nine-month-old WT mice (C57Bl/6) were obtained from the Jackson Laboratory. Mice were housed in groups of three to five on a standard 12 h light/12 h dark cycle, and all experiments were performed during the light cycle. Food and water were provided ad libitum unless otherwise noted. Littermates were randomly assigned to each condition by the experimenter. The experimenter was blind to animal genotypes during tissue processing and electrophysiological recording and analysis. No animals were excluded from analysis.

Adeno-associated viral vectors

Adeno-associated viral (AAV) particles of serotype 5 were obtained from the Vector Core Facility at The University of North Carolina at Chapel Hill. The AAV5 virus contained a channelrhodopsin-2 (ChR2) fused to eYFP in a double-floxed, inverted, open-reading-frame (DIO) driven by the EF1α promoter (Extended Data Fig. 2a). An AAV-DIO–eYFP construct was used as a control.

Surgical procedures

Three-month-old 5XFAD/PV-Cre or CW2 mice were anaesthetized with an intraperitoneal (i.p.) injection of a mixture of ketamine (1.1 mg/kg) and xylazine (0.16 mg/kg). A small craniotomy was made 2.0 mm posterior to bregma and 1.8 mm lateral to the midline on the left side. Virus was delivered through a small durotomy by a glass micropipette attached to a Quintessential Stereotaxic Injector (Stoelting). The glass micropipette was lowered to 1.2 mm below the brain surface. A bolus of 1 μL of virus (AAV-DIO-ChR2–eYFP or AAV-DIO–eYFP; 2 × 1012 viral molecules per millilitre) was injected into the CA1 region of the hippocampus at 0.075 μL min−1. The pipette remained in place for 5 min following the injection before being retracted from the brain. A unilateral optical fibre implant (300 μm core diameter; Thor Labs) was lowered to 0.9 mm below the brain surface about the injection site. Two small screws anchored at the anterior and posterior edges of the surgical site were bound with dental glue to secure the implant in place.

For electrophysiological recordings, adult (3-month-old) male 5XFAD/PV-Cre and 5XFAD negative littermates (for CA1 recordings), or 5XFAD and their WT littermates (for VC recordings) mice were anaesthetized using isoflurane and placed in a stereotactic frame. The scalp was shaved, ophthalmic ointment (Puralube Vet Ointment, Dechra) was applied to the eyes, and Betadine and 70% ethanol were used to sterilize the surgical area. For CA1 recordings, a craniotomy (in millimetres, from bregma: −2 anterior/posterior, 1.8 medial/lateral) was opened to deliver 1 μL of virus to CA1 (as described above). The target craniotomy site for LFP recordings was marked on the skull (in mm, from bregma: −3.23 anterior/posterior, 0.98 medial/lateral for CA1 and 2.8 anterior/posterior, 2.5 medial/lateral for VC), three self-tapping screws (F000CE094, Morris Precision Screws and Parts) were attached to the skull, and a custom stainless steel headplate was affixed using dental cement (C&B Metabond, Parkell). On the day of the first recording session, a dental drill was used to open the LFP craniotomies (300–400 μm diameter) by first thinning the skull until ~100 μm thick, and then using a 30-gauge needle to make a small aperture.

The craniotomy was then sealed with a sterile silicone elastomer (Kwik-Sil WPI) until recording that day and in between recording sessions.

Optogenetic stimulation protocol

Two to four weeks after virus injection and implant placement (which provided time for the mice to recover and undergo behaviour training for animals used for electrophysiology, and the virus to express in the neurons), CA1 neurons were optogenetically manipulated. A 200 mW, 4,793 nm DPSS laser was connected to a patch cord with a fibre channel/physical contact connector at each end. During the experiment, 1 mW (measured from the end of the fibre) of optical stimulation was delivered for 1 h. For molecular and biochemical analyses, each animal received one of three stimulation protocols: 8 Hz, 40 Hz, or random stimulation (light pulses were delivered with a random interval determined by a Poisson process with an average frequency of 40 Hz). eYFP control animals received 40 Hz stimulation. For electrophysiological recordings, each animal received all stimulation conditions interleaved during recordings.

Visual stimulation protocol

Fifteen minutes before the experiment, 5XFAD mice were treated with saline (control) or picrotoxin (0.18 mg/kg)25. For molecular and biochemical analyses, mice were then placed in a dark chamber illuminated by a light-emitting diode (LED) bulb and exposed to one of five stimulation conditions: dark, light, 20 Hz, 40 Hz (12.5 ms light on, 12.5 ms light off, 60 W), 80 Hz flicker for 1h. For electrophysiological recordings, each animal received dark, light, 40 Hz flicker, or random (light pulses were delivered with a random interval determined by a Poisson process with an average interval of 40 Hz) stimulation conditions interleaved in 10 s blocks during recordings.

Behaviour training and virtual reality environment (VR) for electrophysiology

For CA1 recordings, head-fixed animals ran on an 8-inch spherical treadmill supported by an air cushion through a virtual reality environment, as described in ref. 30. The motion of the spherical treadmill was measured by an optical mouse and fed into virtual reality software31, running in MATLAB (version 2013b, Mathworks). The virtual environment consisted of a linear track with two small enclosures at the ends where the animal could turn (Extended Data Fig. 1a). Animals were rewarded with sweetened condensed milk (diluted 1:2 in water) at each end of the track for alternating visits to each end of the track.

Animals learned to run on the virtual linear track over approximately 1 week. The animals were left to recover from the surgery for 1 week, and habituated to handling for 1–2 days before behavioural training began. To learn to manoeuvre on the treadmill and get comfortable in the testing environment, on the first 2 days of training the animals were placed on the spherical treadmill with the virtual reality system off and were rewarded with undiluted sweetened condensed milk. On the second day of training on the spherical treadmill, the animals' food was restricted to motivate them to run. Animals were restricted to no more than 85% of their baseline weight and typically weighed over 88% of their baseline weight. From the third day until the end of training (typically 5–7 days) the animals were placed on the treadmill for increasing amounts of time (30 min to 2 h) running in the VR linear track. Animals were rewarded with diluted (1:2) sweetened condensed milk at the end of the linear track after traversing the length of the track. Between recording sessions, animals were given refresher training sessions to maintain behavioural performance.

For VC recordings, animals ran on the spherical treadmill while exposed to dark, light, or light-flickering conditions (described below in data acquisition). Before recordings, animals learned to manoeuvre on the treadmill and get comfortable in the testing environment by being placed on the spherical treadmill (with the virtual reality system off) and receiving a reward of undiluted sweetened condensed milk.

Electrophysiology data acquisition

For optogenetic stimulation of CA1 during recording, a 300 μm core optical fibre was advanced through the craniotomy used to deliver virus to CA1 to a depth of 900 μm into the brain. Light pulses that were 1 ms and 1 mW (measured from the end of the fibre) were delivered via a 473 nm DPSS (diode pumped solid state) laser (as described above).

To avoid photoelectric artefacts, neural activity was recorded with glass electrodes. LFP electrodes were pulled from borosilicate glass pipettes (Warner) on a filament-based micropipette puller (Flaming-Brown P97, Sutter Instruments), to a fine tip, which was then manually broken back to a diameter of ~10–20 μm and filled with sterile saline. For CA1 recordings the LFP electrode was advanced through the LFP recording craniotomy at an angle 60 degrees posterior to the coronal plane and 45° inferior to the horizontal plane until clear electrophysiological signatures of the hippocampal stratum pyramidale layer were observed (~600–1000 μV theta waves while the animal was running, clearly distinguishable SWRs during immobility, and multiple spikes greater than 150 μV; Extended Data Fig. 1b). For VC recordings, the LFP electrode was advanced vertically through the LFP recording craniotomy to a depth of 600–900 μm and multiple spikes greater than 150 μV were observed.

Data were acquired with a sampling rate of 20 kHz and bandpass filtered 1 Hz to 1 kHz. Animals ran on the spherical treadmill or rested for prolonged periods. For optogenetic simulation sessions, data were recorded for 30 min before any stimulation began. Then stimulation was delivered at gamma (40 Hz), random (as described under Optogenetic stimulation protocol), or theta (8 Hz) frequency for 10 s periods interleaved with 10 s baseline periods (no stimulation). In two animals, stimulation of each type or baseline was delivered for 5 min periods instead of 10 s periods. Each 30 min of stimulation recordings were followed by 5–30 min of recording with no stimulation. For visual light flicker simulation sessions, LED striplights surrounding the animal lights were flickered at gamma (40 Hz), random (described above in Visual stimulation protocol), theta (8 Hz), or 20 Hz frequency for 10 s periods, or were on continuously for 10 s periods, interleaved with 10 s periods with lights off. A few recordings were made above the brain surface during light flicker to ensure that the lights did not create electrical or photoelectric noise during recording. Recording sessions were terminated after approximately 3–5 h. Animals were 3–4 months old at the time of recording.

Spike detection

Spikes were detected by thresholding the 300–6,000 Hz bandpassed signal. Threshold was the median of the filtered signal plus five times a robust estimator of the standard deviation of the filtered signal (median/0.675) to avoid contamination of the standard deviation measure by spikes[32].

LFP

Recorded traces were downsampled to 2 kHz and then bandpass filtered between 1 and 300 Hz.

Theta and SWR detection

Activity across the hippocampal network changes markedly when animals run or sit quietly, and these changes are often referred to as different network states. These network states are clearly distinguishable by the presence or absence of LFP oscillations in different frequency bands[12,13]. When animals ran, we observed large theta (4–12 Hz) oscillations in CA1 as others have shown (Extended Data Fig. 1b, left)[13,30,33,34]. When animals sat quietly, theta oscillations were no longer visible and we recorded SWRs, high-frequency oscillations of 150–250 Hz that last around 50–100 ms and are associated with bursts of population activity, as others have observed (Extended Data Fig. 1b, right)[15,16].

SWRs were detected (Fig. 1a–d and Extended Data Fig. 1d–i) when the envelope amplitude of the filtered trace was greater than four standard deviations above the mean for at least 15 ms. The envelope amplitude was calculated by taking the absolute value of the Hilbert transform of the filtered LFP. We also confirmed our results held when using a higher threshold for SWR detection, six standard deviations above the mean, which detects larger SWRs (Extended Data Fig. 1j, k). To detect theta (Extended Data Fig. 1c, d), the LFP was bandpass filtered for theta (4–12 Hz), delta (1–4 Hz), and beta (12–30 Hz) using an FIR equiripple filter. The ratio of theta to delta and beta ('theta ratio') was computed as the theta envelope amplitude divided by the sum of the delta and beta envelope amplitudes. Theta periods were classified as such when the theta ratio was greater than one standard deviation above mean for at least 2 s and the ratio reached a peak of at least two standard deviations above mean. Non-theta periods were classified as such when the theta ratio was less than one for at least 2 s. SWRs, theta periods, and non-theta periods were visually inspected to ensure that these criteria accurately detected SWRs, theta periods, and non-theta periods, respectively.

Power spectrum

Spectral analysis was performing using multitaper methods (Chronux toolbox, time-bandwidth product = 3, number of tapers = 5). For examining power spectra without stimulation (Extended Data Fig. 1c, d), only theta periods were included: theta periods greater than 5 s long were divided into 5 s trials and the average power spectral density was computed for each animal over these trials. For examining power spectra during optogenetic (Fig. 1e and Extended Data Fig. 1l) and visual stimulation (Fig. 4a and Extended Data Fig. 4a), data were divided into 10 s trials of each stimulation condition or baseline periods, and the average power spectral density was computed for each animal over these trials.

Gamma during SWRs

Spectrograms were computed using multitaper methods (Chronux toolbox). The spectrogram was computed for each SWR including a window of 400 ms before and after the peak of the SWR. Then a z-scored spectrogram was computed in each frequency band using the mean and standard deviation of the spectrogram computed across the entire recording session to create a normalized measure of power in units of standard deviation (Fig. 1a and Extended Data Fig. 1e). Instantaneous frequency of gamma during SWRs was computed by bandpass filtering the LFP for 10–50 Hz, taking the Hilbert transform, then taking the reciprocal of the difference in peaks of the transformed signal (Fig. 1b and Extended Data Fig. 1f). Gamma power before, during, and after SWRs was computed by filtering the LFP for low gamma (20–50 Hz) and taking the amplitude of the envelope of the Hilbert transform to get the mean gamma power in 100 ms bins centred on the SWR peak. This was normalized by the mean and standard deviation of the amplitude of the envelope for the entire recording session to get z-scored gamma power for each bin

around each SWRs (Fig. 1c and Extended Data Fig. 1g, j). Phase modulation by gamma during SWRs was computed by bandpass filtering the LFP for gamma (20–50 Hz), taking the Hilbert transform, and determining the phase of the resulting signal for each spike that occurred during SWRs (Extended Data Fig. 1h). To measure differences in phase modulation between 5XFAD and WT animals, we used resampling with replacement: a subset of 100 spikes from each recording was randomly selected to create a phase modulation distribution and this was repeated 500 times for each recording (Fig. 1d and Extended Data Fig. 1k). We then measured the depth of modulation for the spike-gamma phase distribution by computing the difference between the peak and trough divided by the sum of the peak and trough for each distribution (Fig. 1d and Extended Data Fig. 1k).

Differences in firing during stimulation

To plot stimulus-evoked multiunit firing histograms, spikes were binned in 2.5 ms bins for 100 ms after the start of each light-on pulse and the fraction of spikes in each bin was computed. Mean and standard error were then computed across all light-on periods. To compute differences in multi-unit firing rate between conditions, firing rates were computed for each 10 s period of stimulation or baseline (total number of spikes divided by duration of period). Differences in firing rate were taken between nearby periods of the relevant type of stimulation (firing rate in gamma stimulation period minus baseline or random periods for optogenetic stimulation, firing rate in gamma stimulation period minus baseline, continuous on, or random periods for light flicker stimulation). Differences from all animals were plotted in histograms (Extended Data Figs 1m and 4c) and the median and quartiles of the multiunit firing rates per 40 Hz stimulation, random stimulation, and no stimulation period for each animal were plotted in box plots (Extended Data Figs 1o and 4d).

Immunohistochemistry

Mice were perfused with 4% paraformaldehyde under deep anaesthesia, and the brains were post-fixed overnight in 4% paraformaldehyde. Brains were sectioned at 40 µm using a vibratome (Leica). Sections were permeabilized and blocked in PBS containing 0.2% Triton X-100 and 10% normal donkey serum at room temperature for 1 h. Sections were incubated overnight at 4 °C in primary antibody in PBS with 0.2% Triton X-100 and 10% normal donkey serum. Primary antibodies were anti-EEA1 (BD Transduction Laboratories; 641057), anti-β-amyloid (Cell Signaling Technology; D54D2), anti-Iba1 (Wako Chemicals; 019-19741), anti-parvalbumin (Abcam; ab32895), and anti-Rab5 (Enzo Life Sciences; ADI-KAP-GP006-E). To confirm ELISA experiments, the anti-Aβ antibody D54D2 was used because it allowed for co-labelling with EEA1 and the anti-Aβ antibody 12F4 was used because it does not react with APP, allowing us to determine whether our labelling was specific to Aβ. For co-labelling experiments, the anti-Aβ antibody 12F4 (Biolegend; 805501) was used. Primary antibodies were visualized with Alexa-Fluor 488 and Alex-Fluor 647 secondary antibodies (Molecular Probes), and cell nuclei visualized with Hoechst 33342 (Sigma-Aldrich; 94403). Images were acquired using a confocal microscope (LSM 710; Zeiss) with a 40× objective at identical settings for all conditions. Images were quantified using ImageJ 1.42q by an experimenter blind to treatment groups. For each experimental condition, two coronal sections from at least three animals were used for quantification. Scale bars are 50 µm. For CA1 imaging, the analysis was restricted to the pyramidal cell layer, except in the case of Iba1+ cells analysis, where the whole field of view was required to image an adequate number of cells. ImageJ was used to measure the diameter of Iba1+ cell bodies and to trace the processes for length measurement. In addition, the Coloc2 plugin was used to measure co-localization of Iba1 and Aβ. Imarisx64 8.1.2 (Bitplane, Zurich, Switzerland) was used for three-dimensional rendering. For counting the 'plaque number', deposits of at least 10 µm were

included.

CLARITY

Fixed brains were sliced into 100 µm coronal sections on a vibratome (Leica VT100S) in 1× PBS. Sections containing VC were selected, with reference to the Allen Mouse Brain Atlas, and incubated in clearing buffer (pH 8.5–9.0, 200 mM sodium dodecylsulfate, 20 mM lithium hydroxide monohydrate, 4 mM boric acid in double-distilled H2O) for 2 h, shaking at 55 °C. Cleared sections were washed 3 × 10mins in 1× PBST (0.1% Triton-X100/1XPBS) and put into blocking solution (2% bovine serum albumin/1× PBST) overnight, shaking at room temperature27. Subsequently, three 1 h washes in 1× PBST were performed, shaking at room temperature. Sections were then incubated at 4 °C for 2 days, shaking, with anti-β-amyloid (Biolegend; 805501) and anti-Iba1 (Wako Chemicals; 019-19741) primary antibodies, diluted to 1:100 in 1× PBST. Another set of 3 × 1 h washes in 1× PBST was conducted before sections were incubated for 9 h, shaking at room temperature, in 1:100 1× PBS-diluted secondary antibody mixture. Fragmented Donkey Anti-Rabbit Alexa Fluor 488 (Abcam; ab175694) and Anti-Mouse 568 (Abcam; ab150101) secondary antibodies were used to visualize the primary antibody labelling. Halfway through this incubation period, Hoechst 33258 (Sigma-Aldrich; 94403) was spiked into each sample at a 1:250 final dilution. Sections were then washed overnight in 1× PBS, shaking at room temperature. Before mounting for imaging, slices were incubated in refractive index matching solution (75 g Histodenz, 20 mL 0.1 M phosphate buffer, 60 mL double-distilled H2O) for 1 h, shaking at room temperature. Tissue sections were mounted onto microscopy slides with coverslips (VWR VistaVision, VWR International, LLC, Radnor, Pennsylvania, USA) using Fluromount G Mounting Medium (Electron Microscopy Sciences, Hatfield, Pennsylvania, USA). Images were acquired on a Zeiss LSM 880 microscope with the accompanying Zen Black 2.1 software (Carl Zeiss Microscopy, Jena, Germany). Section overview and cellular-level images used for three-dimensional reconstruction were taken using a Plan-Apochromat 63×/1.4 oil differential interference contrast objective. Imarisx64 8.1.2 (Bitplane, Zurich, Switzerland) was used for three-dimensional rendering and analysis.

Western blot

CA1 whole-cell lysates were prepared using tissue from 3-month-old male 5XFAD/PV-Cre mice. Tissue was homogenized in 1 ml RIPA (50 mM Tris HCl pH 8.0, 150 mM NaCl, 1% NP-40, 0.5% sodium deoxycholate, 0.1% SDS) buffer with a hand homogenizer (Sigma), incubated on ice for 15 min, and rotated at 4 °C for 30 min. Cell debris was isolated and discarded by centrifugation at 14,000 r.p.m. for 10 min. Lysates were quantitated using a nanodrop, and 25 µg protein was loaded on a 10% acrylamide gels. Protein was transferred from acrylamide gels to PVDF membranes (Invitrogen) at 100 V for 120 min. Membranes were blocked using bovine serum albumin (5% w/v) diluted in TBS:Tween. Membranes were incubated in primary antibodies overnight at 4 °C and secondary antibodies at room temperature for 90 min. Primary antibodies were anti-APP (Invitrogen; PAD CT695), anti-APP (Sigma; A8967), and anti-β-actin (Abcam; ab9485). Secondary antibodies were horseradish peroxidase-linked (GE Healthcare). Signal intensities were quantified using ImageJ 1.46a and normalized to values of β-actin. We examined tau protein solubility using sequential protein extraction as described in ref. 28. We then probed the detergent insoluble tau fraction using an antibody against Tau5 (Thermo Fisher Scientific; AHB0042).

ELISA

CA1 or VC was isolated from male mice, lysed with PBS or 5M Guanidine HCl, and subjected to Aβ

measurement with the use of mouse (for WT experiments) or human (for all other experiments) Aβ1–40 or Aβ1–42 ELISA kit (Invitrogen) according to the manufacturer's instructions. We lysed the tissue in phosphate-buffered saline (PBS) to extract the PBS soluble Aβ fraction. The soluble Aβ fraction probably contained monomeric and oligomeric Aβ. Tissue was further treated with guanidine HCl to extract the insoluble Aβ fraction. Aβ1–42 was below detectable levels for both flicker and control groups in WT VC and microglia-specific samples.

Genome-wide RNA-seq

Total RNA was extracted from CA1 isolates using the RNeasy kit (Qiagen). Purified mRNA was used for RNA-seq library preparation using the BIOO NEXTflex kit (BIOO 5138-08) according to the manufacturer's instructions. Total mRNA (1 μg) was subject to a sequential workflow of poly-A purification, fragmentation, first strand and second strand synthesis, DNA end-adenylation, and adaptor ligation. The libraries were enriched by 15 cycles of PCR reactions and cleaned with Agencourt AMPure XP magnetic beads (Beckman Coulter). The quality of the libraries was assessed using an Advanced Analytical-fragment Analyzer. The bar-coded libraries were equally mixed for sequencing in a single lane on the Illumina HiSeq 2000 platform at the MIT BioMicro Center. The raw fastq data of 50-bp single-end sequencing reads were aligned to the mouse mm9 reference genome using TopHat2.0. The mapped reads were processed by Cufflinks 2.2 with UCSC mm9 reference gene annotation to estimate transcript abundances, and test for differential expression. An average of 26,518,345 sequencing reads was obtained from three stimulated and three non-stimulated mice. Relative abundance of transcript was measured by fragments per kilobase of exon per million fragments mapped (FPKM). Gene differential expression test between treated and untreated groups was performed using Cuffdiff module with an adjusted P value <0.05 for statistical significance (GEO accession number GSE77471).

To understand the cellular and molecular mechanisms from our RNA-seq data, 14 of publicly available RNA-seq datasets[35] were processed for cell-type-specific analysis. Additionally, 60 publicly available neuron-, microglia-, and macrophage-specific RNA-seq datasets under different chemical and genetic perturbations[36,37,38,39,40,41] were downloaded and processed using TopHat/Cufflinks pipeline for gene set enrichment (GSEA) statistical analysis. GSEA was used to determine whether a defined gene set from our RNA-seq data are significantly enriched at either direction of a ranked gene list from a particular perturbation study. Genes detected in the public RNA-seq datasets were ranked by log2 values of fold change (case versus control), from positive to negative values. A defined gene set (in our case, up- or downregulated genes upon gamma treatment) was considered significantly correlated with a perturbation-induced transcriptomic change (either up- or downregulation) when both nominal P value and false discovery rate q value were less than 0.05. The sign of the calculated normalized enrichment score (NES) indicates whether the gene set is enriched at the top or the bottom of the ranked list. The heatmap for differentially expressed genes was generated using a custom R script, and z-score values across all libraries for each gene were calculated on the basis of the gene FPKM values. The box plots for cell-type specificity analysis were also generated by the R program, on the basis of gene FPKM values.

Quantitative RT–PCR

The CA1 subregion was isolated from hippocampus of 3-month-old male 5XFAD/PV-Cre mice. Tissue was rapidly frozen using liquid nitrogen and stored at −80 °C, and RNA extracted using the RNeasy kit according to the manufacturer's protocol (Qiagen). RNA (3 μg) was treated with DNase I (4 U, Worthington Biochemical Corporation), purified using RNA Clean and Concentrator-5 Kit (Zymo Research) according

to the manufacturers' instructions, and eluted with 14 µL DEPC-treated water. For each sample, 1 µg RNA was reverse transcribed in a 20 µL reaction volume containing random hexamer mix and Superscript III reverse transcriptase (50 U, Invitrogen) at 50 °C for 1 h. First strand cDNAs were diluted 1:10 and 1 µL were used for RT-qPCR amplification in a 20 µL reaction (SsoFast EvaGreen Supermix, Bio-Rad) containing primers (0.2 µM). Relative changes in gene expression were assessed using the $2^{-\Delta\Delta Ct}$ method.

Isolation of microglia from VC

The primary VC (V1 region) was rapidly dissected and placed in ice-cold Hanks' balanced salt solution (HBSS) (Gibco by Life Technologies, catalogue number 14175-095). The tissue was then enzymatically digested using the Neural Tissue Dissociation Kit (P) (Miltenyi Biotec, catalogue number 130-092-628) according to the manufacturer's protocol, with minor modifications. Specifically, the tissue was enzymatically digested at 37 °C for 15 min instead of 35 min and the resulting cell suspension was passed through a 40 µm cell strainer (Falcon Cell Strainers, Sterile, Corning, product 352340) instead of a MACS SmartStrainer, 70 µm. The resulting cell suspension was then stained using allophycocyanin (APC)-conjugated CD11b mouse clone M1/70.15.11.5 (Miltenyi Biotec, 130-098-088) and phycoerythrin (PE)-conjugated CD45 antibody (BD Pharmingen, 553081) according to the manufacturer's (Miltenyi Biotec) recommendations. FACS was then used to purify CD11b and CD45 positive microglial cells. The cells were sorted directly into 1× PBS (Extended Data Fig. 6a).

Code availability

Code is publicly available upon request from the corresponding author.

Statistics

For electrophysiological data that were not normally distributed, results are presented as medians and quartiles unless otherwise noted. Two-sided Wilcoxon rank sum tests for equal medians were performed to determine whether distributions were significantly different, and Wilcoxon signed rank tests were performed to determine whether distributions were significantly different from zero as these do not assume data are normally distributed. Variability was similar between the groups that were statistically compared. The Bonferroni method was used to correct for multiple comparisons. No statistical method was used to estimate sample size, but it was consistent with previous publications.

Molecular and biochemical results are presented as mean + s.e.m. Percentages stated are group means. All statistical analysis used Prism GraphPad software. Normality was determined using the D'Agostino and Pearson omnibus normality test. Variability was similar between the groups that were statistically compared. Comparison data for normally distributed data consisting of two groups were analysed by two-tailed unpaired t-tests. Comparison of normally distributed data consisting of three or more groups was by one-way ANOVA followed by Tukey's multiple comparisons test. Comparisons for non-normally distributed data were performed using Mann–Whitney tests. The statistical test, exact P values, and sample size (n) for each experiment are specified in the figure legend. For optogenetic ELISA data, two-sided unpaired Student's t-tests were performed to compare mice from the same litter that received different conditions. No statistical method was used to estimate sample size, but it is consistent previous publications. Molecular and biochemical analysis used a minimum of three biological replicates per condition.